Journal of Optoelectronics and Advanced Materials Vol. 3, No. 3, September 2001, p. 655 - 664

TRANSIENT PHOTOCURRENT TECHNIQUES AS A MEANS OF CHARACTERISING AMORPHOUS SEMICONDUCTORS

C. Main, D. Nesheva[a]

University of Abertay Dundee, Bell Street, Dundee DD1 1HG, UK.
[a]Institute of Solid State Physics, Bulgarian Academy of Sciences
Boul. Tzarigradsko chaussee 72, Sofia 1784, Bulgaria

We describe techniques to study electronic transport and localized state distributions in amorphous semiconductors from their photocurrent response to steady and impulse excitation. The response to impulse excitation contains information on distributions of trapping and release times for localized states in the mobility gap of the material; the problem is to determine a unique density of states (DOS) from such data. One technique is applicable to cases in which both trapping and release processes are significant. A second 'post-transit' analysis is restricted to situations where only carrier release processes are significant. In both cases we derive analytical DOS spectroscopies capable of fine energy resolution. We also report on studies of transport and DOS distributions, in thin films of several representative chalcogenides, including recent studies of surface defect states in CdSe nanocrystals in SiO_x matrix. We also report on interpretation of steady state and transient measurements on thin film amorphous As_2Se_3.

(Received June 25, 2001; accepted September 3, 2001)

Keywords: Transient photocurrent, Amorphous chalcogenides, CdSe nanocrystals

1. Introduction

In 'transient photocurrent' experiments, a semiconductor is excited with a short pulse of light, and the photocurrent response *i(t)* is measured. Two possibilities are discussed below. The first is the transient photocurrent (TPC) experiment in which a gap-cell is used, with ohmic contacts. The second is the post – transit experiment in which a high reverse field is applied to non-injecting contacts on 'sandwich' device. Either method may be used to determine the energy distribution of various species of gap states which influence carrier mobilities and lifetimes in the semiconductor, under the assumption that the response is controlled by multi-trapping processes. A reliable method would represent a valuable diagnostic tool for material quality.

The TPC method avoids extraction of charge at contacts, and the response may be considered to be a complex function of trapping and release involving the whole ensemble of localised states, and also recombination processes [1]. On the other hand, the post-transit response is a much simpler process, determined only by the collection of charge being released from successively deeper traps [2,3]. Thus the analytical approaches to determination of the gap-state distribution are necessarily very different.

Recently there has been much interest in the electronic transport and optical properties of semiconductor nanoparticles, in particular CdSe nanocrystals in SiO_x/CdSe multilayer and composite SiO_x-CdSe films [4,5]. Defect states in these films have been studied by sub-band absorption and thermally stimulated currents. It would be very useful to complement such studies using the ability of TPC to probe a wide energy range in a single measurement. In this study, we report on preliminary work on such materials.

Work on steady state and transient photoconductivity in amorphous As_2Se_3 has been reported by the author [6,7] and others [8]. Such measurements have been interpreted as revealing a broad featureless exponential tail of states above the valence band mobility edge (TPC) [9], or in contrast, a fairly well defined set of recombination centres in the gap [7]. In this paper, we return to the topic, in the light of the more recent findings from TPC analysis methods, in an attempt to reconcile these differences, perhaps speculatively.

2. DOS spectroscopy

2.1 TPC Theory

A continuous *g(E)* may be represented by a finely spaced ladder of *m* discrete levels, of spacing δE and density $N_{ti} = g(E_i)\delta E$. The basic multi-trapping equations are,

$$\frac{dn(t)}{dt} = -\sum_{i}^{m} \frac{dn_{ti}(t)}{dt} - \omega_R n(t) + N_0 \delta(t), \tag{1}$$

and

$$\frac{dn_{ti}(t)}{dt} = -\omega_{ei} n_{ti}(t) + \omega_{ti} n(t), \tag{2}$$

where *n(t)* is the free carrier density at time *t*, $n_{ti}(t)$ is the instantaneous trapped carrier density at the ith level localized state below the mobility edge, ω_R is the recombination rate constant, N_0 is the initial generated excess density, ω_{ei} [= $n\exp(-E_{ti}/kT)$] is the release rate constant and ω_{ti} [= $vsg(E_{ti})dE$] is the capture rate constant for the ith localized state. Energy $E_{ti} = i\delta E$ is the depth of the ith level, ν is the attempt to escape frequency, *s* is the capture cross-section and *v* is the thermal velocity.

Applying a Fourier transform to Eqs. (1) and (2), gives in the frequency domain,

$$\hat{n}(\omega) = \int_0^\infty n(t)[\cos(\omega t) - j\sin(\omega t)]dt = \frac{N_0}{(A_\omega + jB_\omega)}, \tag{3}$$

where, treating the density of states (DOS) as continuous in energy,

$$A_\omega = \omega_R + \int_0^{E_f} v\sigma g(E)\left(1 + \exp\left(-\frac{2(E_\omega - E)}{kT}\right)\right)^{-1} dE \tag{4}$$

and

$$B_\omega = \frac{i(0)\sin(\varphi(\omega))}{\left|\hat{I}(\omega)\right|} = \omega + \int_0^{E_f} \frac{v\sigma}{2}\, g(E)\,\mathrm{sech}\left(\frac{E_\omega - E}{kT}\right)dE. \tag{5}$$

In the above, $\hat{I}(\omega)$ represents the frequency domain photocurrent associated with $\hat{n}(\omega)$, *i(0)* is the initial value of the transient photocurrent – *i.e.* when all N_0 excess carriers are free, and E_f is the Fermi energy. The term *k* is Boltzmann's constant, and *T* is the absolute temperature.

Eq. (5) is a Fredholm integral equation of the first kind, and is 'ill-conditioned'. A simple *approximate* solution used by the authors [10] replaces the peaked sech function with a delta function, to give

$$g(E) \approx \frac{2}{v\sigma\pi kT}\left(\frac{i(0)\sin(\varphi(\omega))}{\left|\hat{I}(\omega)\right|} - \omega\right). \tag{6}$$

This approximation results in an effective '*kT* broadening' effect – see section 3.1 below. More rigorous solutions for the analogous integral equation obtained by Laplace transformation have been attempted by Gueorguieva *et al.* [11], Naito and co-workers, using specialized techniques such as Tikhonov regularization [12, 13]

In our proposed approach, the high-resolution FT method (HFT) we convert Eq. (5) back to a summation over a fine ladder $g(E_{tj})\Delta E$ of discrete traps, to give,

$$\frac{i(0)\sin(\varphi(\omega))}{\left|\hat{I}(\omega)\right|} - \omega = \sum_j \frac{v\sigma}{2}\, g(E_{tj})\Delta E\,\mathrm{sech}\left(\frac{E_\omega - E_{tj}}{kT}\right). \tag{7}$$

The left hand side of Eq. (7) represents information obtained from experiment, although *i*(0) may not be observable in practice. The discrete array of energies $E_{tj} = j\Delta E$ need not coincide with the original E_{ti} above. The magnitude of the second term ω, is not significant in the frequency range encountered experimentally. The right side, with the DOS implicit in a summation, is obtained from

multi-trapping theory. In our proposed HFT method, we solve Eq. (7) for $g(E_{tj})$, fitting the right side of Eq. (7) to the experimental data, whilst *retaining* the sech function of Eq. (5). We use a finely spaced set of model functions, $A_j \frac{\nu\sigma}{2} \Delta E\,\mathrm{sech}\left(\left(E_\omega - E_{tj}\right)/kT\right)$, with a general least-squares fitting technique LMDIF1 [14], where the A_j [$= g(E_{tj})$] are the adjustable fitting parameters. Specific values of w are selected at intervals to give equi-spaced E_ω [$= kT \ln(\nu/\omega)$], over the related energy range. In general a very good fit for the amplitude parameters A_j and hence $g(E_{tj})$ may be obtained, with overall standard error values of < 1%.

We note that the analysis performed on Eq. (7) does not require knowledge of the recombination constant ω_R, and hence the recombination time t_R [$=1/\omega_R$]. The important consequence of this is that the proposed analysis can be applied to *i(t)* data which span both pre- and post-recombination (or post-transit) time regimes.

2.2 'Post – Transit' theory

Fig. 1 compares the computed relative distribution of excess trapped charge in an exponential band-tail under conditions with no extraction (*pre-transit*) and with extraction (*post-transit*), after the same elapsed time (10^{-4} s) from initial excitation. The sharp variation in occupation in the latter case presents the possibility of improvement in resolution, over the methods of the previous section.

We consider again that the continuous density of states may be represented by a very fine ladder of discrete trapping levels N_{ti} , i = 1,2... m, at associated energies E_i. Of the initial excess electron density N_0 introduced by pulsed excitation, a fraction N' is trapped, and the remainder is removed by collection, so that

$$N' = N_0 \frac{t_0}{t_0 + \tau_t}, \tag{8}$$

where t_0 is the transit time of free electrons and t_t is the trapping time into the ensemble of traps, of total density N_T. The initial trapped fraction $n_{ti}(0)$ is distributed according to the density of trapping states, assuming an energy-independent capture coefficient, so we may write for the trapped electron distribution

$$n_{ti}(0) = N_{ti} N'/N_T \, . \tag{9}$$

In the post-transit situation, the multi-trapping rate equation for free electron density n reduces to

$$\frac{dn}{dt} = \sum_i n_{ti}(t)\nu \exp\left(\frac{E_i}{kT}\right) - \frac{n}{t_0}, \tag{10}$$

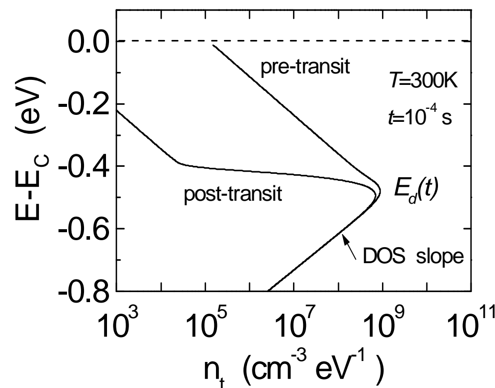

Fig.1 Computed distributions at time 10^{-4} s after excitation, of excess trapped charge in an exponential band - tail of characteristic energy 50 meV, for pre - transit and post-transit cases. The sharp edge in occupation caused by trap - stripping in the post-transit case is evident.

where the summation is necessarily only over deep-lying states whose combined trapping time is greater than the transit time. Retrapping terms are considered by definition to be negligible, so we can also write

$$n_{ti}(t)=n_{ti}(0)\exp\left(-\frac{t}{\tau_i}\right), \tag{11}$$

where t_i is the average thermal release time from states at level i.

The solution to Eq. 10 is

$$n(t)=n(0)\exp\left(-\frac{t}{t_0}\right)+\sum_i n_{ti}(0)\nu\exp\left(\frac{E_i}{kT}\right)\frac{\exp\left(-\frac{t}{\tau_i}\right)-\exp\left(-\frac{t}{t_0}\right)}{1/t_0-1/\tau_i}, \tag{12}$$

which under post-transit conditions (t, $t_i >> t_0$), gives to a good approximation,

$$i(t)=e\mu\mathcal{E}An(t)\approx e\mu\mathcal{E}A\sum_i n_{ti}(0)\frac{t_0}{\tau_i}\exp\left(-\frac{t}{\tau_i}\right), \tag{13}$$

where e is the electronic charge, μ is the electron mobility, $\mathcal{E}$ is the applied field, and A is the conduction cross sectional area of the sample. At this point, the 'standard' analysis [2] converts the summation to an integral over a continuous distribution, to the form of a Laplace transform, and replaces the exponential trap release time distribution factor in Eq. (13) with a delta function $t_i\,\delta(t-t_i)$. This approximation is equivalent to the assumption that all traps at a given depth release at the same time. The result is

$$g(E)\approx t\,i(t)\left(\frac{N_T}{N'e\mu\mathcal{E}At_0kT}\right). \tag{14}$$

The *alternative* proposed here, is to *retain* the trap release time distribution function of Eq. (13) and simply perform a *fit* to the photocurrent *i(t)* of Eq. (13), with a finely spaced set of model functions, $(A_j/\tau_j)\exp(-t/\tau_j)$, again using the least-squares fitting technique LMDIF1 [14], where the set A_j are the adjustable fitting parameters. Values of t_j are pre-selected so that the energy range covered is appropriate to the time range of the *i(t)* data set. Normally values are again chosen to give a uniform spacing ΔE ($< kT$) between levels on the energy scale. We note that since the distribution of states is assumed to be continuous, the choice of t_j is arbitrary, and thus not necessarily identical to t_i, as long as the energy spacing is very close ($< kT$). In general a very good fit may be obtained, with overall standard error value of < 1%. The amplitude parameters A_j are equated with $e\mu\mathcal{E}An_{tj}(0)$ giving the HPT result,

$$g(E_j)\approx A_j\left(\frac{N_T}{N'e\mu\mathcal{E}At_0\Delta E}\right), \tag{15}$$

for the density of states at energy E_i.

2.3. Experimental

Preliminary TPC measurements have been made on SiO_x/CdSe multilayer and composite SiO_x - CdSe films (x ~ 1.5) having varying CdSe sublayer thicknesses and average nanocrystal sizes. The total film thickness is about 0.2 μm for the multilayers and 1.5 μm for the composite films. The samples were fabricated as sublayers from SiO_x and CdSe on Corning 7059 glass substrates by thermal evaporation of powdered CdSe and granular SiO from two independent sources. Details of the films, preparation, charge transport measurements and structure are given in earlier publications [4,5]. Coplanar sputtered gold electrodes about 10mm long, with 1 mm gaps were deposited on the surface of the samples.

The TPC measurements were made using applied voltages of 100V – 500V, and a temperature range of 293 – 423 K. A nitrogen pumped dye laser (Laser Science VSL-337) was used to produce photogeneration pulses of width 4ns at a wavelength of 500 nm. Incident photon densities were approximately 10^{14} cm^{-2}. Special purpose wideband DIFET current-mode op-amp circuits were used to process the sample current, the decay curves presented in this work being composites of the response at several instrumental bandwidths. The current data were sampled and averaged using a fast digitizing oscilloscope (Tektronix TDS3052), before storage and processing by PC. The transient

current component *i(t)* was calculated by subtracting the steady state current I_{SS} sampled immediately prior to each laser firing. Time was allowed for relaxation between each firing.

We note that any calculation of a 'density of states' from the TPC data obtained in this way will at present only result in an effective DOS for the sample as a whole. However, the relative energy profile of gap states is returned, and this should be of use in determining film quality, and in studying the effects of structural variation.

3. Results and discussion

3.1. TPC simulation

To evaluate the HFT method, we computed the *i(t)* response to impulse excitation for several representative distributions of traps, using a numerical procedure developed by the authors [9]. We then performed a numerical Fourier transform on *i(t)* to obtain $\hat{I}(\omega)$, and calculated the density of states using a fitting procedure with Eq. (7). In addition to this comparison, we calculated the density of states from the *i(t)* data, using the approximate expression of Eq. (6).

In Fig. 2, we show the computed *i(t) vs t* on log – log axes, at temperature 300K for exponential tail distributions with a range of characteristic slope energies E_{ct}, from 50 meV down to 10 meV. This covers cases in which the distribution is broader than kT (25 meV) to those in which the distribution is much narrower than kT.

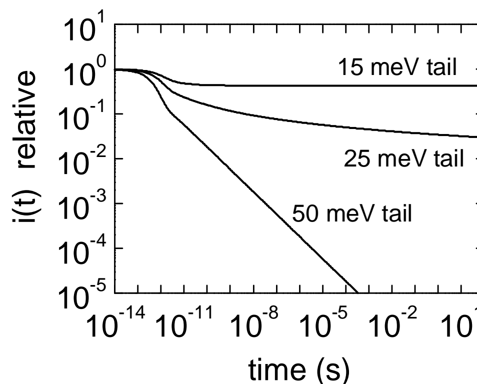

Fig. 2. Simulated transient photocurrent decays for exponential band-tails of various characteristic energies. Simulation temperature 300K.

The broad distribution, E_{ct} = 50 meV results in an *i(t)* which follows the well known power law form $i(t) \propto t^{-(1-\alpha)}$ where $\alpha = kT/E_{ct}$. It is often assumed that such a power law automatically indicates the existence of an exponential band-tail, but this is not necessarily true, as we show below.

In Fig. 3, we display the DOS distributions obtained using the approximate FT method of equation 6, and our precise method of equation 7. It can be seen that the approximate method cannot reproduce the DOS in cases where the tailing is steep, i.e. where $E_{ct} < kT$. In such cases, the method returns a spurious DOS with characteristic energy broadened to a value of about *kT*. On the other hand, our high-resolution HFT method can recover the DOS quite well, even when the tail energy is much less than *kT*.

In Fig. 4, we show the reproduced *g(E)* when the original distribution is a steep exponential tail of characteristic energy E_0 = 35 meV, with superimposed, a sharp Gaussian feature peaking at E_b = 0.3 eV of form $g_b(E) = D\exp\left(-\left((E - E_b)/E_1\right)^2\right)$. The energy E_1 = 25 meV (FWHM = 41.6 meV) and the the factor D is chosen to give a peak 100 times the background tail density at the center of the feature. Now we see the '*kT* broadening' of the approximate FT method, which almost obscures any structure, while the HFT method follows the original density well on both sides of the Gaussian feature.

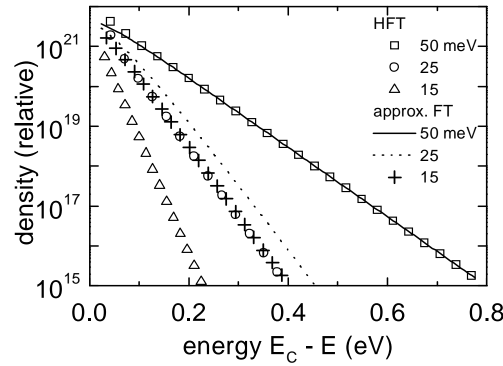

Fig.3 Density of states *g(E)* recovered from computed *i(t)* at 290K,for three exponential tails, Comparison of FT and HFT methods. Note: the HFT method returns a DOS of the correct slope., while the FT method fails for slopes < kT.

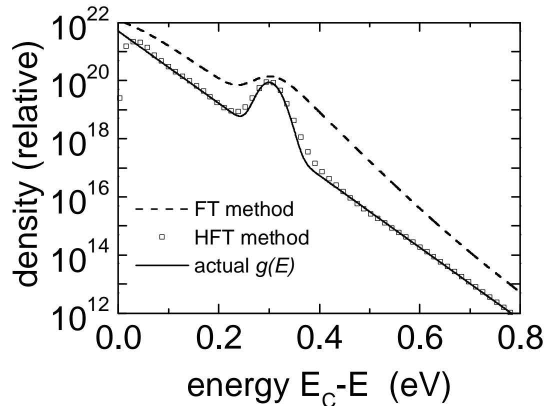

Fig. 4. Density of states *g(E)* recovered from computed *i(t)* at 290K, for an exponential tail, with a sharp Gaussian feature. Comparison of FT and HFT methods.

In Fig. 5, we test the method using two *discrete* levels of equal density, 1.0×10^{17} cm^{-3}, at depths 0.3 and 0.5 eV, flanking a *third* discrete level of *lower* density, 1.0×10^{16} cm^{-3} at 0.4 eV depth. We note that the discrete levels are represented now by a *g(E)* distribution, which when integrated should represent the same total density. The approximate FT method results in broadening, of FWHM = 67 meV (~2.6 *kT*) obscuring the presence of the low density middle level, and introducing also a spurious band-tailing effect closer to the band edge. It is clear that the HFT method gives a much sharper reproduction, FWHM = 27 meV (~ *kT*) also allowing ready identification of the centre level.

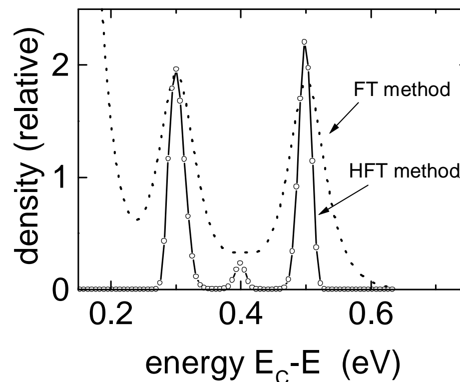

Fig. 5. Density of states *g(E)* recovered from computed *i(t)* at 290K, for Two discrete levels at 0.3 and 0.5 eV depth flanking a third discrete level of 1/10 density at 0.4 eV depth Comparison of FT and HFT methods.

3.2. Post – transit simulation

To evaluate the proposed method, we computed the *i(t)* response under post-transit conditions for several representative distributions of traps, using the numerical procedure mentioned in 3.1, ensuring that the value of t_0 in the simulation was short enough to include any important features in the trap distribution within the post-transit time regime. We then calculated the density of states from the *i(t)* data using the relations of Eq. (14) and Eq. (15) respectively. In addition to this comparison, we calculated the density of states from *pre-transit i(t)* data for the same representative distributions, using the basic FT method described in 2.1. We note that the FT method also involves a delta function approximation to simplify an integration, and so is also subject to a broadening effect.

In Fig. 6, we show the reproduced *g(E)* when the original distribution is the same steep exponential tail with superimposed, sharp Gaussian feature, as in section 2.2 above. The very substantial broadening of the FT method is evident, particularly at energies below the Gaussian peak. The approximate post-transit expression of Eq. (14), is significantly better, as expected. However, the HPT method proposed in the present work follows the original density well, including the Gaussian feature, with a fit which is rather better than the HFT result shown in Fig. 4.

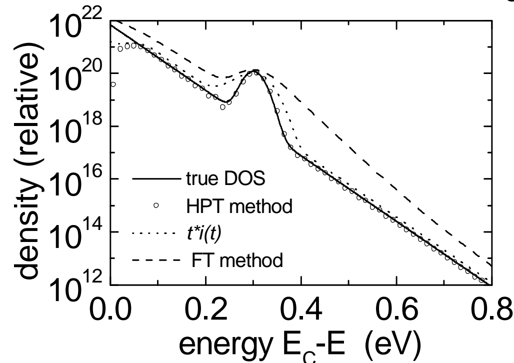

Fig. 6. DOS recovered from computed *i(t)* at 290K for an exponential tail of characteristic energy E_0= 35 meV, with a sharp Gaussian feature at 0.3 eV with FWHM = 41.6 meV. Comparison of approximate and proposed post transit analyses and FT method.

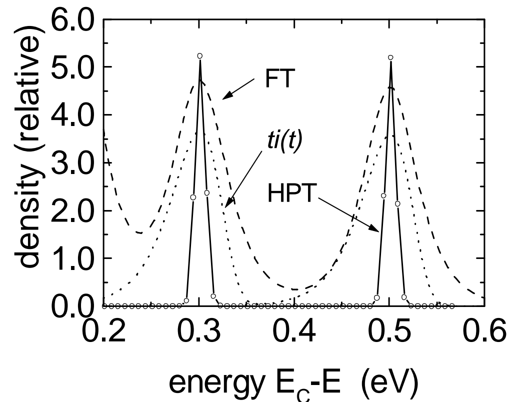

Fig. 7. Density of states recovered from computed *i(t)* at 290K for two discrete trap levels at 0.3 and 0.5 eV depth. While both approximate methods exhibit some *kT* broadening in the recovered DOS, the proposed post - ransit analysis resolves the levels as sharp features, upon a very low noise base.

Next the extreme case is considered of a DOS consisting of two *discrete* levels of equal density, 1.0×10^{17} cm^{-3}, at depths 0.3 and 0.5 eV. Computing the DOS from *i(t)* curves gives the results shown in Fig. 7, where we have scaled the results to ease comparison. We note that the discrete levels are represented now by a *g(E)* distribution, which when integrated should represent the same total density. The symmetrical broadening is evident in the FT method, which gives, as before, a FWHM of 67 meV (2.6 *kT*) while the approximate post-transit analysis is only marginally sharper, and asymmetrically broadened. At the shallow energy side of the recovered DOS for each level,

broadening is evident, similar to that of the FT method, while the deep energy side is rather sharper in form as expected from the observations of Fig. 1. This is a consequence of fitting the asymmetric exponential release time distribution function with a delta function. It is clear however, that the proposed HPT method gives a much sharper and symmetrical reproduction, with FWHM estimated as ~12 meV, or 0.48 *kT* in this case.

3.3. Experimental - multilayers

Fig. 8 shows measured TPC in a multilayer SiO_x(10nm)/CdSe(10nm) film. At 293 K and 323K the *i(t)* decay displays a clear power-law form $i(t) \propto t^{-(1-\alpha)}$, over several decades of time, after an iinitial faster short-time fall at about 100ns. At 293K the slope index (1-a) is –0.75, which might be (wrongly) interpreted as arising from a broad exponential tail of characteristic energy E_{ct} = 100 meV. At 423 K a further feature appears at longer times, which is as yet unexplained.

Fig. 9 shows the relative DOS computed from the *i(t)* data, for all three temperatures. Also shown is a line with slope representing a characteristic energy of 100 meV. The DOS appears to be a broad, almost flat, distribution, over several tenths on an eV. It is evident also that the distribution is far from an 100 meV tail predicted from the power law of the i(t) decay. This is a striking and surprising result at first sight, but a similar effect has been observed experimentally by the authors in other materials, such as a-Si:H, and also discussed in detail, with the aid of simulations [14]. Essentially the departure from the expected exponential DOS form arises from the contribution of the short – time 'pre-power-law' section of *i(t)* to the relevant Fourier integral. Although the highest resolution is not required for this case, we note that application of the simple *approximate* result of equation (6) produced a calculated DOS with a spurious band tail of slope energy equal to *kT* in the range 0.2 – 0.4 eV depth.

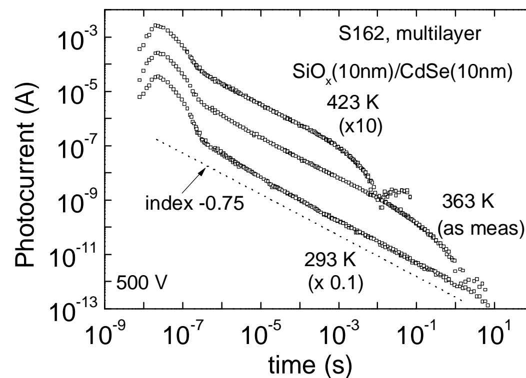

Fig. 8. TPC in a multilayer SiO_x(10nm)/CdSe (10nm) film at 293 K, 363 K and 423 K. Excitation: 4ns pulsewidth, 500 nm, 10^{14} photons cm^{-2} incident. Power law of index – 0.75 is shown.

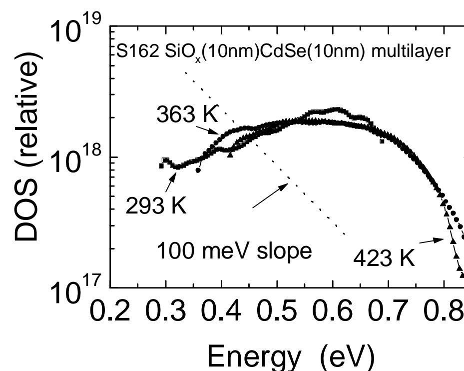

Fig. 9. DOS calculated from TPC data of Figure 8. Also shown is expected tail slope of 100 meV, expected (incorrectly) from the power law observed at 293 K in Fig. 8.

Similar results have been obtained from TPC measurements on composite SiO_x - CdSe films, where we had hoped to identify defect states observed in TSC measurements. Further work is needed to access by TPC, the energy range related to these states.

3.4. Experimental - arsenic triselenide

TPC in As_2Se_3 is normally manifested as a featureless decay in *i(t)*, following a power law over many decades of time, with typically an index of –0.5, at room temperature [9]. This usually leads to an interpretation involving an extensive and featureless exponential tail (above the valence band), On the other hand, As_2Se_3 exhibits bimolecular *steady state* photoconductivity, which has a reasonably well defined activation energy of 0.33 eV [7]. A simple analysis involving valence alternation pair defect centres with negative correlation energy then would 'place' such defects (in the doubly-negative charged state) at around double this value – 0.66 eV into the gap. These two interpretations seem to be incompatible. We speculate here that there may well be some structure in the defect DOS, which peaks at 0.66 eV above the mobility edge. We believe that it has become evident from the present study, and a previous study on a-Si:H, that a power law decay of i(t) over many decades of time, may not be incompatible with DOS distributions which are other than exponential. Further work on this is required.

4. Conclusions

We have shown that simple analytical procedures may be applied to the photocurrent decay observed in the general TPC case and to post-transit pulse photocurrent data to reveal the density of localized states with high resolution. The work shows that the resolution obtained is not limited by *kT* broadening effects. The broadening associated with earlier methods arises because of the approximation of a distribution function, using a delta function, in order to simplify an integral. The best resolution is provided by the new post-transit analysis, while both new methods exhibit versatility in handling cases with either distributed traps or with discrete traps. This means that they can be applied to disordered materials or to crystalline materials with well-defined defect levels.

Experimental results on multilayer SiO_x/CdSe films, indicate a very broad flat energy distribution of localized states exists in the material. The spatial location of such states is not identified by the method, but they may be associated with both the nanoparticle-nanoparticle and nanoparticle-matrix interfaces. The results also demonstrate the pitfalls associated with interpreting a power law TPC in terms of an exponential band-tail. This point was further used in speculating that the power-law TPC decay usually observed in As_2Se_3 films may not in fact indicate a featureless exponential distribution of states, and may not be incompatible with some defect structure in the DOS.

Acknowledgments

The authors acknowledge the Royal Society for financial support via a joint collaboration grant. One of the authors (CM) also acknowledges EPSRC for financial support through research grant GR/M 16696, which allowed development of the analytical methods.

References

[1] C. Main, Proc. MRS Symposium A, Vol. **467**, Eds. M. Hack, E. A. Schiff, S. Wagner, A. Matsuda, R. Schropp, MRS, Warrendale PA, 1997, Ch.143, p.167.
[2] G. F. Seynhaeve, R. P. Barclay, G. J. Adriaenssens, J. M. Marshall, Phys. Rev. B, **39**, 10196 (1989).
[3] S. Usala, G. J. Adriaenssens, Ö. Öktu, M.Nesladek, Appl. Surface Science, **50**, 265 (1991).
[4] D. Nesheva, Z. Levi, Z. Aneva, V. Nikolova, H. Hofmeister, J. Phys.:Condens. Matter., **12**, 751 (2000).
[5] D. Nesheva, Z. Levi, V Pamukchieva, J. Phys.: Condens. Matter., **12**, 3967 (2000).
[6] C. Main, D. P. Webb, R Brüggemann et al, J. Non Cryst. Solids, **137,** 951 (1991).

[7] C. Main, A. E. Owen, Electronic and Structural Properties of Amorphous Semiconductors, Eds. P. G. LeComber, J. Mort, Academic Press, London (1972).
[8] M. Hammam, G. J. Adriaenssens, W Grevendonk, J. Phys. C: Solid State ,**18,** 2151 (1985).
[9] D. Monroe, M. A. Kastner, Phys Rev B, **33**, 8881 (1986).
[10] C. Main, R. Brüggemann, D. P. Webb, S. Reynolds, Solid State Commun., **83**, 401 (1992).
[11] M. J. Gueorguieva, C. Main, S. Reynolds, Proc. MRS Symposium A, Volume 609, Eds. R. W. Collins, H.M. Branz, S. Guha, H. Okamoto, M. Stutzmann, MRS, Warrendale PA, 2000.
[12] T. Nagase, K. Kishimoto, H. Naito, J. Appl. Phys. **86**, 5026 (1999).
[13] N. Tikhonov, A. V. Goncharsky, V. V. Stepanov, A. G. Yagola, Numerical Methods for the Solution of Ill-Posed Problems, Kluwer Academic Publishers, Netherlands (1995).
[14] S. Garbow, K. E. Hillstrom, J. J. More, Argonne National Laboratory MINPACK Project (1980).
[15] C. Main, R. Brüggemann, D. P. Webb et al., J. Non-Cryst Solids, **166**, 481 (1993).
[16] C. Main, R. Brüggemann, Electronic and Optoelectronic Materials for the 21st Century, Eds. N Kirov, A Vavrek, World Scientific Press,Singapore ,1993, p. 270.